

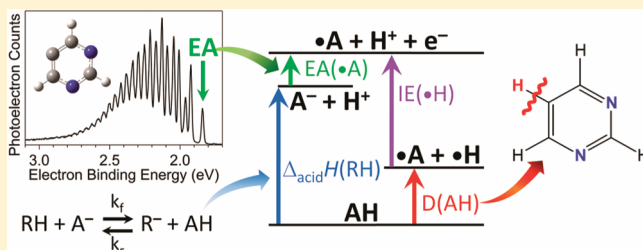
C–H Bond Strengths and Acidities in Aromatic Systems: Effects of Nitrogen Incorporation in Mono-, Di-, and Triazines

Scott W. Wren, Kristen M. Vogelhuber, John M. Garver,[†] Shuji Kato, Leonid Sheps,[‡] Veronica M. Bierbaum,* and W. Carl Lineberger*

JILA and Department of Chemistry and Biochemistry, University of Colorado, 440 UCB, Boulder, Colorado 80309, United States

Supporting Information

ABSTRACT: The negative ion chemistry of five azine molecules has been investigated using the combined experimental techniques of negative ion photoelectron spectroscopy to obtain electron affinities (EA) and tandem flowing afterglow-selected ion tube (FA-SIFT) mass spectrometry to obtain deprotonation enthalpies ($\Delta_{\text{acid}}H_{298}$). The measured $\Delta_{\text{acid}}H_{298}$ for the most acidic site of each azine species is combined with the EA of the corresponding radical in a thermochemical cycle to determine the corresponding C–H bond dissociation energy (BDE). The site-specific C–H BDE values of pyridine, 1,2-diazine, 1,3-diazine, 1,4-diazine, and 1,3,5-triazine are 110.4 ± 2.0 , 111.3 ± 0.7 , 113.4 ± 0.7 , 107.5 ± 0.4 , and 107.8 ± 0.7 kcal mol^{−1}, respectively. The application of complementary experimental methods, along with quantum chemical calculations, to a series of nitrogen-substituted azines sheds light on the influence of nitrogen atom substitution on the strength of C–H bonds in six-membered rings.



INTRODUCTION

There has been increasing interest in understanding the pyrolysis of nitrogen-containing heterocycles, especially five-membered (azole) and six-membered (azine) compounds.^{1–3} These nitrogen-rich species are abundant in coal^{4,5} and represent the fundamental unit of many high-energy-density materials.^{6,7} Combustion of these compounds leads to the production of nitrogen oxide (NO_x) species, which play an important role in the formation and degradation of tropospheric ozone.⁸ A number of studies have focused on the pyrolysis of azine molecules containing one, two, and three nitrogen atoms (referred to as pyridine, diazines, and triazines, respectively).^{9–14} One of the main goals of these studies was to determine the strength and reactivity of specific C–H bonds that were shown to be critical in the decomposition process. For example, the generally accepted mechanism for decomposition of pyridine is initiated by the cleavage of the weakest C–H bond—the bond adjacent to the nitrogen atom.³ Clearly, knowledge of the bond dissociation energy (BDE) of various C–H bonds in azine molecules is needed to elucidate the decomposition pathways of high-energy materials.

Knowledge of the C–H bond strengths of azines is critical to the modeling community. Experimental bond strength values provide data points with which theoreticians can compare their models. However, few experimental studies of gaseous azines exist, and they have been largely limited to shock tube experiments that rely on complex modeling of the data, resulting in fairly large error bars.^{9,11,12,14–16} Moreover, to date there are no experimental determinations of the BDEs of 1,2-diazine or any triazines. The experimental shock tube results

were later complemented by a comprehensive theoretical investigation by Barckholtz et al. focused on computing the C–H and N–H BDEs of aromatic hydrocarbons.¹⁷ The goal of their study was to identify a practical and adequate computational method for calculating properties of molecules that can approximate the network nature of coal. The experimental C–H bond strengths reported in this work provide highly accurate data points to test decomposition models and computational methods.

In addition, azines are relevant biologically and in synthetic chemistry.¹⁸ Azines are involved in the catalysis of biological and chemical systems and in oxidation–reduction reactions of enzymes in living systems. Present in vitamins and in nicotine, they provide the basis for thousands of pharmaceuticals. Fundamental understanding of acidities and bond strengths in aromatic systems is of central relevance to modern methods in synthetic organic chemistry, including *ortho*-metalation,¹⁹ cross-coupling,²⁰ amination,²¹ and C–H functionalization.^{22,23} Azines also serve as building blocks of supramolecular chemistry.¹⁸

Azines are also interesting from a fundamental standpoint because they are model systems to investigate how replacement of a C–H group with a nitrogen atom affects the thermochemical properties of six-membered aromatic rings. By systematically replacing a C–H group with N, we evaluate competing intramolecular effects that influence all fields of chemistry. The previous shock tube and theoretical studies found that in cases with more than one possible C–H bond

Received: October 11, 2011

fission site, the most stable radical site was always adjacent to a nitrogen atom. Furthermore, both experimental and theoretical studies found that the strength of all C–H bonds in pyridine and the diazines were lower than the C–H bond strength in benzene (112.9 ± 0.5 kcal mol⁻¹), the prototypical six-membered ring aromatic molecule.²⁴ Here we identify two predominant factors—an inductive effect assisted by resonance and electron lone-pair repulsion—that affect the gas-phase acidities and EAs of various sites of the azines.

In this report we use a combination of gas-phase ion chemistry, anion photoelectron spectroscopy, and *ab initio* calculations to investigate the deprotonation enthalpies, radical EAs, and C–H bond strengths of five azine molecules: pyridine, 1,2-diazine (pyridazine), 1,3-diazine (pyrimidine), 1,4-diazine (pyrazine), and 1,3,5-triazine (s-triazine). We measure the EA of the azinyl radical corresponding to deprotonation of the most acidic site. The location of that site is determined unambiguously through a combination of simulation of the full photoelectron spectrum, H–D exchange kinetics, and *ab initio* calculations. The ion–molecule reactor is used to determine the gas-phase acidity of this site for each azine (with the exception of pyridine,¹⁵ which has been measured previously). With these values, we determine the C–H BDE of the most acidic deprotonation site in each azine molecule, using a well-established thermochemical cycle.²⁵ Due to the large number of molecules studied, as well as the similarity of analyses for all of these azines, we organize the experimental results into six sections. To illustrate the analysis performed for all molecules studied here, we present a detailed analysis of 1,3-diazine, which typifies the azine compounds in the present work, and limit ourselves to an overview of the other four azines studied (additional plots and detailed analyses of the other azines can be found in Supporting Information). Following the experimental results, we discuss the general trends in C–H bond strengths observed in the context of progressively adding nitrogen atoms to azines.

■ EXPERIMENTAL METHODS

Negative Ion Photoelectron Measurements. The negative ion photoelectron spectrometer used in this experiment has been described in detail previously.²⁶ The apparatus consists of four main sections: an ion source, mass spectrometer, laser with build-up cavity, and electron energy analyzer. Negative ions are formed in a flowing afterglow ion source. A microwave discharge containing trace amounts of O₂ in He buffer gas (~0.4 Torr) generates atomic oxygen radical anion, O⁻. Methane is added downstream of O⁻ formation, and H-atom abstraction from methane forms hydroxide (HO⁻), which is thermalized and subsequently reacts with an appropriate azine precursor (pyridine, 1,2-diazine, 1,3-diazine, 1,4-diazine, 1,3,5-triazine: ≥97%, Sigma-Aldrich) to generate azinide anions. As an example, the reaction of pyridine with HO⁻ leads to deprotonation of the azine: HO⁻ + C₅H₅N → C₅H₄N⁻ + H₂O. Since many of the azine molecules have low vapor pressures, high-purity helium (General Air, 99.999%) is bubbled through the sample, which significantly increases the azinide ion signal. Collisions with He buffer gas vibrationally cool the product anions to ~300 K. The flow tube can be further cooled with a liquid nitrogen jacket to make a cold anion beam, which has a vibrational temperature near 150 K. The photoelectron spectra of 1,3-diazinide and 1,3,5-triazinide were recorded at 150 K; cooling the flow tube often results in a significant loss of ion current, and we were unable to produce sufficient ion currents to collect “cold spectra” of the remaining azinides. However, cold spectra are not needed to identify the origin peaks of the azinyl radicals, nor do they allow for a more precise determination of the EA. Anions are extracted into a differentially pumped region and accelerated to 735 eV before

entering a Wien velocity filter with a mass resolution of $m/\Delta m \approx 60$. The mass-selected ion beam (typically 50–120 pA) is decelerated to 35 eV and focused into the laser interaction region. Here, the ~1 W output from a single-mode continuous-wave argon ion laser operating at 364 nm (3.40814 eV) is built up to ~100 W of circulating power in an actively stabilized optical buildup cavity located within the vacuum system. The laser beam and the ion flight axis intersect, producing photoelectrons by direct detachment. Electrons ejected into a small solid angle orthogonal to both the laser and ion beams enter a hemispherical energy analyzer, and the transmitted portion of the photoelectron energy distribution is imaged onto a position-sensitive detector. Multiple overlapping photoelectron energy ranges are merged into a complete spectrum, providing the distribution of photoelectrons as a function of kinetic energy. The energy resolution of the analyzer is ~11 meV under the experimental conditions used here.

By subtracting the measured electron kinetic energy (eKE) from the photon energy, we obtain the electron binding energy (eBE) spectrum. The absolute energy scale is calibrated²⁶ before and after each experiment using the well-known EA of oxygen atom.²⁷ Additionally, the energy scale is corrected for a slight linear compression (<1%)²⁶ using the photoelectron spectrum of O₂⁻, which provides a number of known transitions spanning the 0.5–3.0 eV photoelectron energy range.²⁸ After making these corrections and accounting for the resolution of the spectrometer and rotational peak profiles, absolute electron binding energies can be determined with an accuracy of 5 meV or better.²⁶ A rotatable half-wave plate positioned outside the buildup cavity controls the polarization of the photo-detachment radiation. When the angle between the laser polarization and the electron collection direction is 54.7°, the “magic angle”, the recorded spectrum is independent of variations in the photoelectron angular distributions.²⁹ Therefore, the photoelectron intensities collected at the magic angle are directly proportional to the total photodetachment cross section. All spectra shown here were collected with magic angle polarization. Simulation of the full magic angle photoelectron spectrum allows (in each case presented here) determination of the site(s) where deprotonation occurred.

Flowing Afterglow-Selected Ion Flow Tube (FA-SIFT) Measurements. The corresponding gas-phase acidities of the azines are determined via proton-transfer reaction kinetic measurements using a variety of anions in a tandem FA-SIFT instrument that has been described previously.^{30,31} Reactant anions are formed in a flowing afterglow source, mass selected by a quadrupole mass filter, and injected into the reaction flow tube where they thermally equilibrate with a helium buffer gas (0.5 Torr, 298 K) before undergoing proton-transfer reactions with a neutral reagent. All reagents were obtained commercially and were purified by several freeze–pump–thaw cycles. Primary anions were prepared in the first (source) flow tube by 70 eV electron impact on N₂O or NH₃, producing O⁻ or NH₂⁻ by dissociative attachment. Subsequent reaction of O⁻ with methane results in formation of HO⁻. The additional reactant anions employed (azinides or CH₃O⁻) are generated in the source flow tube using HO⁻ deprotonation of the corresponding neutral species. The ions are mass selected and injected into a second (reaction) flow tube at low injection energies (typically at $E_{\text{lab}} = 20$ eV) to minimize fragmentation. The neutral reagent is added through inlets located at varying distances downstream along the flow tube. Rate constants are determined from the depletion of the reactant ion signal recorded with a detection quadrupole mass filter coupled to an electron multiplier. Absolute uncertainties in the rate measurements are ±20%. Product branching ratios are determined by extrapolating the observed product yields to zero reaction distance in order to extract the intrinsic ratios due to primary reactions. Mass discrimination for ions of different masses is accounted for by tuning the detection system with known anion standards. No further corrections are made in the analysis.

The gas-phase acidity measurements for the most acidic proton of the azines (AH) are made relative to a reference acid (RH) by measuring the forward (k_f) and reverse (k_r) proton-transfer reaction rate constants at 298 K, shown below in eq 1.



The ratio of the rate constants gives the proton-transfer equilibrium constant ($K_{\text{equil}} \equiv k_f/k_r$), which can then in turn be used with the known $\Delta_{\text{acid}}G_{298}(\text{RH})$ to determine $\Delta_{\text{acid}}G_{298}(\text{AH})$ using eq 2.

$$\Delta_{\text{acid}}G_{298}(\text{AH}) = \Delta_{\text{acid}}G_{298}(\text{RH}) + RT \ln K_{\text{equil}} \quad (2)$$

Methanol [$\Delta_{\text{acid}}G_{298}(\text{CH}_3\text{OH}) = 375.5 \pm 0.6 \text{ kcal mol}^{-1}$]²⁴ is the reference acid for 1,2-diazine (Aldrich, 98%), 1,3-diazine (Aldrich, 99%), and 1,3,5-triazine (Aldrich, 97%), while water [$\Delta_{\text{acid}}G_{298}(\text{H}_2\text{O}) = 383.68 \pm 0.02 \text{ kcal mol}^{-1}$]²⁴ is used for 1,4-diazine (Aldrich, >99%). The enthalpy of deprotonation ($\Delta_{\text{acid}}H_{298}$) can be obtained from the measured $\Delta_{\text{acid}}G_{298}(\text{AH})$ using eq 3, where the entropy of deprotonation ($\Delta_{\text{acid}}S_{298}$) is determined from electronic structure calculations.³²

$$\Delta_{\text{acid}}H_{298}(\text{AH}) = \Delta_{\text{acid}}G_{298}(\text{AH}) + T\Delta_{\text{acid}}S_{298}(\text{AH}) \quad (3)$$

The rate constants for reactions of the azinide anions with neutral reactants were measured by injecting the anions and monitoring the ion intensity as a function of reactant inlet position (i.e., reaction distance); neutral reactant flow rates were measured using a calibrated volume system. The error bars for these measurements represent one standard deviation from the mean of the data. For the reverse reactions involving the neutral azines as reactants, an alternate approach was employed since the azines have low volatility and flow measurements are difficult. For example, to measure the rate constant for reaction of methoxide with 1,2-diazine and 1,3-diazine, a stable flow of the diazine entrained in helium is allowed to react with hydroxide ion. The highly exothermic proton-transfer reaction for this reference anion is assumed to occur at $90 \pm 10\%$ reaction efficiency, based on extensive previous data. The reactivity of methoxide is then measured relative to that of hydroxide, using the same flow of diazine, and the absolute rate constant is thereby determined. A similar approach was employed to measure the rate constant for reaction of hydroxide with 1,4-diazine, where the highly exothermic proton-transfer reaction of amide with 1,4-diazine was used as the reference. This general approach has been used successfully for the acidity measurements of azoles,^{33,34} and the final error bars reflect the additional assumptions of the method. It was possible to measure the flow rate of 1,3,5-triazine with the calibrated volume system; thus the absolute rate constant for the reaction of methoxide with 1,3,5-triazine was determined directly.

The reported reaction efficiencies are determined by dividing the experimental rate constants by the calculated collision rate constants ($\text{Eff} = k_{\text{expt}}/k_{\text{col}}$). The parametrized trajectory collision rate theory³⁵ that is used to calculate k_{col} requires knowledge of the electric dipole moment and the scalar polarizability of the neutral reactant. The polarizability and electric dipole moment of CH_3OH and H_2O are taken from the literature.³⁶ The polarizabilities of 1,2-diazine, 1,3-diazine, 1,4-diazine, and 1,3,5-triazine are calculated using the method of Miller and Savchik³⁷ to be 5.58-, 8.58-, 8.58-, and $7.73 \times 10^{-24} \text{ cm}^3$, respectively. The electric dipole moments of 1,2-diazine and 1,3-diazine are reported to be 4.22 and 2.334 D, respectively,³⁶ while by symmetry 1,4-diazine and 1,3,5-triazine have zero electric dipole moments.

Reactivities of the azinides, including pyridinide (generated using 99.8% pyridine from Aldrich), are examined by reacting the anions with D_2O (for H/D exchange), H_2O and CH_3OH (for proton transfer). Methoxide deprotonation is also used to generate anions of 1,3-diazine and 1,3,5-triazine, which are injected into the second flow tube for reactivity studies.

Theoretical Methods. Electronic structure calculations were performed with the Gaussian 03 software package.³⁸ Geometry optimization and frequency calculations were carried out using the density functional theory (DFT) method with Becke's hybrid three-parameter functional³⁹ and the correlation functional of Lee et al.⁴⁰ (B3LYP) and with an augmented correlation-consistent polarized double- ζ basis set (aug-cc-pVDZ).^{41,42} No scaling factor is applied to the calculated vibrational frequencies. Single point electronic energies

are also calculated using the B3LYP/aug-cc-pVTZ and MP4(SDQ)/6-31+G(d) levels of theory on stationary point geometries obtained from B3LYP/aug-cc-pVDZ and B3LYP/6-311++G(d,p), respectively.

The Franck–Condon profiles of the photoelectron spectra are simulated using the PESCAL program.⁴³ The simulations employ the calculated geometries, normal mode vectors, and vibrational frequencies of the anion and neutral states. The Franck–Condon factors are computed in the harmonic oscillator approximation including Duschinsky rotation using the Sharp–Rosenstock–Chen method.⁴⁴ The individual vibronic peak contours are simulated by a Gaussian function with a fwhm of 11 meV, consistent with instrumental resolution.

RESULTS

Figure 1 shows the negative ion photoelectron spectra of the five azinide anions studied, as well as the previously published

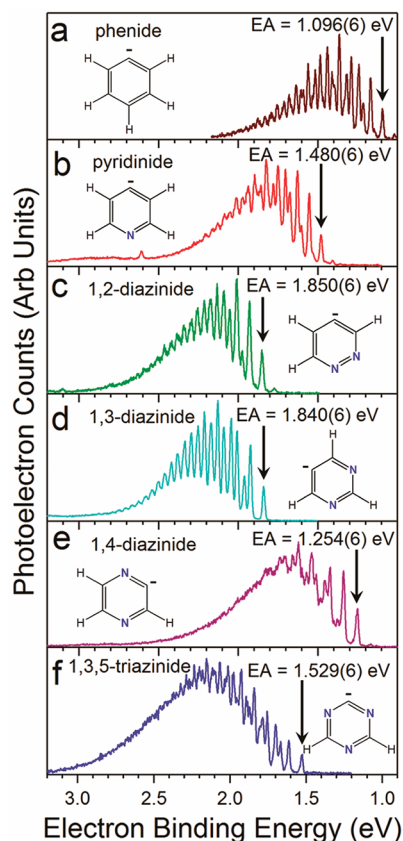
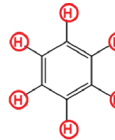
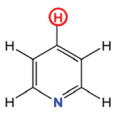
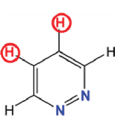
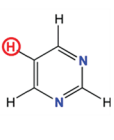
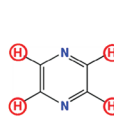
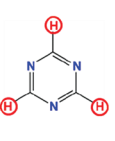


Figure 1. Magic-angle negative ion photoelectron spectra of (a) phenide, (b) pyridinide, (c) 1,2-diazinide, (d) 1,3-diazinide, (e) 1,4-diazinide, and (f) 1,3,5-triazinide.

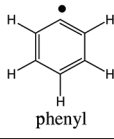
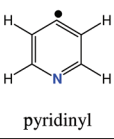

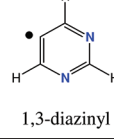
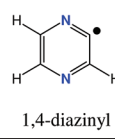

spectrum of phenide⁴⁵ for comparison. The indicated deprotonation site for each species was determined experimentally as described in the Detailed Results and Analysis section. All spectra show extensive vibrational progressions in the ground electronic state of the neutral radical species, and one of the most striking features of the azinide spectra is the similarity of these vibrational progressions. The structure in the spectra is largely dominated by two ring-distortion vibrational modes with frequencies of ~ 700 and 1000 cm^{-1} , analogous to those observed in the phenide spectrum.⁴⁵ As illustrated above, the remarkable similarity of the photoelectron spectra is a consequence of the very similar ring distortions that occur upon electron photodetachment from the azinide anions.

Table 1. Summary of Experimental Thermochemical Properties of Azines Reported Here: C–H Bond Dissociation Energies, Electron Affinities, and Deprotonation Enthalpies^a

						
	benzene	pyridine	1,2-diazine	1,3-diazine	1,4-diazine	1,3,5-triazine
$D_{298}(\text{C-H})$ (kcal mol ⁻¹)	112.9 ± 0.5 ^b	110.4 ± 2.0	111.3 ± 0.7	113.4 ± 0.7	107.5 ± 0.4	107.8 ± 0.7
EA (eV)	1.096 ± 0.006 ^c	1.480 ± 0.006	1.850 ± 0.006	1.840 ± 0.006	1.254 ± 0.006	1.529 ± 0.006
$\Delta_{\text{acid}}H_{298}(\text{C-H})$ (kcal mol ⁻¹)	401.2 ± 0.5 ^b	389.9 ± 2.0 ^d	382.2 ± 0.7	384.6 ± 0.7	392.2 ± 0.4	386.1 ± 0.7

^aThe site to which the thermochemical data refers is indicated by a circled, red H. ^bReference 24. ^cReference 45. ^dReference 15.

Table 2. Experimental Vibrational Frequencies (cm⁻¹) of Azinyl Radicals and Anions^a

						
	phenyl	pyridinyl	1,2-diazinyl	1,3-diazinyl	1,4-diazinyl	1,3,5-triazinyl
Neutral ^b	$\nu_{9/10}=968 \pm 15$	$\nu_7=1010 \pm 50$	$\nu_{12/13}=1000 \pm 80$	$\nu_7=980 \pm 20$	$\nu_{12/13}=980 \pm 80$	$\nu_{4/5}=1110 \pm 70$
Neutral ^c	$\nu_4=600 \pm 10$	$\nu_9=600 \pm 20$	$\nu_{14}=640 \pm 20$	$\nu_8=680 \pm 20$	$\nu_{14}=700 \pm 20$	$\nu_7=680 \pm 20$
Anion ^c	NA	$\nu_9=580 \pm 50$	$\nu_{15}=620 \pm 50$	$\nu_8=660 \pm 40$	$\nu_{14}=670 \pm 50$	$\nu_7=670 \pm 40$

^aFrequencies are labeled on the basis of mode ordering for a particular azine; complete list in Tables S1–S5. ^bSymmetric in-plane ring *breathing* motion of atoms illustrated in Chart 1. ^cSymmetric in-plane ring *distorting* motion of atoms illustrated in Chart 1.

Table 3. Summary of FA-SIFT Results

azine	reaction	kinetic data			thermochemistry ^a			anion H/D exchange with D ₂ O ^b
		<i>k</i> _{proton transfer} ^c	Eff ^d		Δ _{acid} G ₂₉₈	TΔ _{acid} S ₂₉₈ ^e	Δ _{acid} H ₂₉₈	
pyridine	H ₂ O + C ₅ H ₄ N [−] HO [−] + C ₅ H ₅ N	— —	— —		382.1 ± 2.0 ^e	7.9	389.9 ± 2.0 ^f	2 H/D (4-anion; 3,5-exchange)
1,2-diazine	CH ₃ OH + 1,2-C ₄ H ₃ N ₂ [−] CH ₃ O [−] + 1,2-C ₄ H ₄ N ₂	<i>k</i> _f <i>k</i> _r	2.2 ± 0.4 28 ± 6	0.11 0.64	374.0 ± 0.7	8.2	382.2 ± 0.7	3 H/D (4-anion; 3,5,6-exchange)
1,3-diazine	CH ₃ OH + 1,3-C ₄ H ₃ N ₂ [−] CH ₃ O [−] + 1,3-C ₄ H ₄ N ₂	<i>k</i> _f <i>k</i> _r	12 ± 2 1.3 ± 0.3 ^g	0.63 0.05	376.8 ± 0.7	7.8	384.6 ± 0.7	2 H/D (5-anion; 4,6-exchange)
1,4-diazine	H ₂ O + 1,4-C ₄ H ₃ N ₂ [−] HO [−] + 1,4-C ₄ H ₄ N ₂	<i>k</i> _f <i>k</i> _r	7.2 ± 2 9.3 ± 2	0.31 0.51	383.5 ± 0.4	8.7	392.2 ± 0.4	3 H/D (all four sites equivalent)
1,3,5-triazine	CH ₃ OH + C ₃ H ₂ N ₃ [−] CH ₃ O [−] + C ₃ H ₃ N ₃	<i>k</i> _f <i>k</i> _r	11 ± 2 0.55 ± 0.20	0.53 0.04	377.3 ± 0.7	8.8	386.1 ± 0.7	2 H/D (all three sites equivalent)

^aUnits of kcal mol⁻¹. ^bAnion site; exchange positions. ^cUnits of 1 × 10⁻¹⁰ cm³ s⁻¹. ^dReaction efficiency is proton-transfer rate constant relative to the collision rate constant using parametrized trajectory rate theory. ^eCalculated at the B3LYP/6-311++G(d,p) level of theory. ^fReference 15. ^gRate constants adjusted for possible ring-open structures.

Each spectrum has a clear origin peak (the 0 ← 0 transition) that is marked with an arrow indicating the measured EA, reported in Table 1. The pyridinide (1b), 1,2-diazinide (1c), and 1,4-diazinide (1e) spectra collected at 300 K exhibit a single hot band peak to the lower-eBE side of the origin peak. From these hot bands, we extract a frequency corresponding to a transition originating from an excited ring-distortion mode in the anion. Measured vibrational frequencies are summarized in Table 2. With the photon energy of 3.40814 eV, we do not observe clear spectroscopic signatures of excited electronic states of the neutral radicals. There are weak features that appear at higher binding energy in the spectra of pyridinide and

1,2-diazinide, but the data do not allow for a conclusive assignment.

Table 3 summarizes the results of the gas-phase acidity measurements from the FA-SIFT experiments. Our experimental acidities refer to the most acidic sites in the azines, all of which fall within an 8 kcal mol⁻¹ range and have error bars of less than 1 kcal mol⁻¹. The reactions used to study 1,2-diazine and 1,4-diazine, shown in Table 3, proceed almost exclusively via proton transfer with negligible formation of adducts or byproducts in either the forward or reverse directions. However, byproducts in the reactions of 1,3-diazine and 1,3,5-triazine require the use of product-ion branching ratios to

determine the reverse proton-transfer rate constant. In a detailed study, Schafman and Wenthold recently measured the gas-phase acidity of the *ortho*, *meta*, and *para* sites of pyridine, taking great care to identify the deprotonation site.¹⁵ Because the acidity measurement is complicated by the issue of the regioselectivity of pyridine deprotonation, we would not have been able to improve upon their results and therefore did not attempt to repeat these measurements. However, preliminary experiments undertaken in our laboratory are consistent with their results. To obtain the C–H bond strength of pyridine with the smallest error bar, we use the value reported by Schafman et al.

Using the measured EA and $\Delta_{\text{acid}}H$ values, we directly determine the BDE at 298 K for all five azines via the thermochemical cycle²⁵ depicted in Figure 2. The

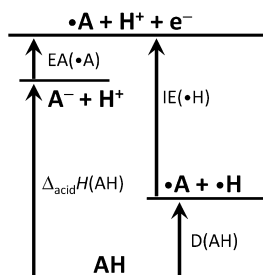


Figure 2. Schematic of the negative ion thermochemical cycle used to obtain the C–H BDEs, $D(\text{AH})$, in this work. $\text{IE}(\text{H})$ is the well-known ionization energy of a hydrogen atom; $\Delta_{\text{acid}}H$ is the deprotonation enthalpy of the neutral molecule AH ; $\text{EA}(\text{A})$ is the electron affinity of the corresponding radical species.

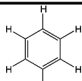
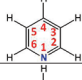
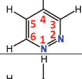
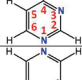
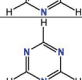
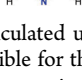
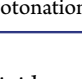
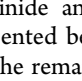
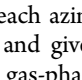
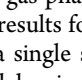
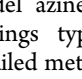
$\Delta_{\text{acid}}H_{298}(\text{AH})$ is obtained at 298 K, but we must correct the EA and ionization of the hydrogen atom, $\text{IE}(\text{H})$ —which are measured at 0 K—by the integrated heat capacities to determine the BDE at 298 K, as shown in eq 4:⁴⁶

$$D_{298}(\text{A–H}) = \Delta_{\text{acid}}H_{298}(\text{AH}) + \text{EA}_0(\text{A}) - \text{IE}_0(\text{H}) + \int_0^{298} \Delta C_p(T) dT \quad (4)$$

where $D(\text{A–H})$ is the BDE and $\Delta_{\text{acid}}H(\text{AH})$ is the gas-phase enthalpy of deprotonation. In the present work, we apply this well-established methodology to obtain the C–H bond strengths of the most acidic sites of several azines. The resulting BDEs are reported in Table 1. Due to the accuracy of our EA and gas-phase acidity measurements, our site-specific C–H BDEs have much smaller error bars than the previously reported values for pyridine, 1,3-diazine, and 1,4-diazine. The BDEs of 1,2-diazine at the 4-position and of 1,3,5-triazine are experimentally determined for the first time.

As discussed in the Experimental Methods section, the azinide anions are made in both experiments by deprotonation of the parent azine using HO^- . In the case of 1,4-diazine and 1,3,5-triazine, all hydrogen atoms are equivalent, and there is only one anion isomer possible. However, for pyridine, 1,2-diazine, and 1,3-diazine, there are several unique hydrogen atoms, each with a different gas-phase acidity. We identify the deprotonation site by comparing the experimental photoelectron spectra with Franck–Condon simulations of the different possible isomers, as well as comparing the measured EA and $\Delta_{\text{acid}}H$ values with calculations, given in Table 4. We justify our assignment of the pyridinide, 1,2-diazinide, and 1,3-

Table 4. Calculated^a EAs, $\Delta_{\text{acid}}H_{298}$ Values, and $D(\text{C–H})$ for Benzene and the Azines^b

	$\Delta_{\text{acid}}H_{298}$ (kcal mol ⁻¹)	EA (eV)	$D(\text{C–H})$ (kcal mol ⁻¹)
 benzene	399.2	1.095	110.9
 pyridine(2)	399.4	0.854	105.5
 pyridine(3)	391.8	1.433	111.3
 pyridine(4)	389.7	1.469	110.0
 1,2-diazine(3)	389.8	1.342	107.1
 1,2-diazine(4)	380.5	1.819	108.9
 1,3-diazine(2)	396.2	1.072	107.3
 1,3-diazine(4)	389.4	1.251	104.7
 1,3-diazine(5)	383.7	1.824	112.2
 1,4-diazine	391.0	1.224	104.7
 1,3,5-triazine	385.4	1.500	106.4

^aCalculated using B3LYP/aug-cc-pVDZ. ^bIf more than one isomer is possible for the anion/radical, the number in parentheses indicates the deprotonation site.

diazinide anion isomers individually in the following results presented below.

The remainder of the Results section is organized as follows: for each azine molecule studied, we identify the deprotonation site and give a brief summary of the photoelectron spectrum and gas-phase acidity measurements. Due to the similarity of the results for the five azines compounds, we first focus in detail on a single species: 1,3-diazine. We selected 1,3-diazine as the model azine because it highlights the major challenges and findings typical of the azine/azinide/azinyl systems. The detailed methodology described for 1,3-diazine is representative of that employed for all of the following azines. We then present summarized results of the remaining azines: pyridine, 1,2-diazine, 1,4-diazine, and 1,3,5-triazine. The complete set of simulations for all azines reported here appear in Supporting Information (Figures S1–S5), along with thorough explanations of isomer assignments for those species with multiple possible deprotonation sites.

Detailed Experimental Results and Analysis for a Representative Azine: Negative Ion Photoelectron Spectrum of 1,3-Diazine. The 150 K, magic-angle photoelectron spectrum of 1,3-diazinide is shown in Figure 3, along with Franck–Condon spectral simulations of the three possible 1,3-diazinide isomers. To assess the relative abundance of these three isomers in our data we rely on both photoelectron spectroscopy and thermochemical measurements. The structure and extent of a photoelectron spectrum is determined by the geometry change that takes place upon photodetachment, allowing identification of the anion isomer by its spectral “fingerprint”.^{47–49} To facilitate comparison of the predicted spectral features of each isomer with the observed spectrum, all simulations are shifted so that they share the experimental origin (i.e., each simulation is shifted by the difference in eBE between the measured EA and the calculated EA of that isomer). The proximity of the N atom to the deprotonation site influences the EA of the various isomers, and we compare the measured EA to the calculated EA for additional proof of which isomer is observed in the spectrum.

As Figure 3 indicates, the simulated photoelectron spectra of 1,3-diazinide isomers differ significantly. The simulation of 1,3-

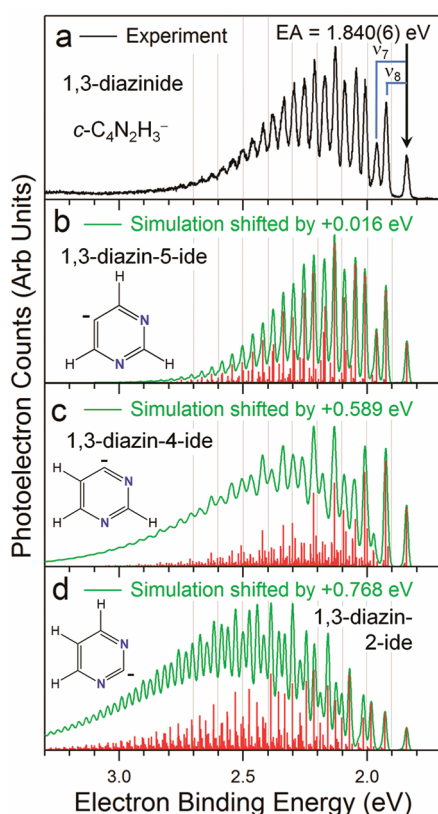


Figure 3. Magic-angle negative ion photoelectron spectrum of 1,3-diazinide: (a) 364-nm experimental spectrum of ions cooled to ~ 150 K. Peaks used to identify vibrational frequencies are indicated with solid blue lines. Simulated 150 K photoelectron spectra of (b) 1,3-diazin-5-ide, (c) 1,3-diazin-4-ide, and (d) 1,3-diazin-2-ide are shown in green. Each simulation has been shifted by the difference between the experimental EA and the calculated EA of each isomer such that all simulations are plotted at the measured origin.

diazin-5-ide has nearly quantitative agreement with the experimental photoelectron spectrum, while neither the vibrational structure nor the calculated EA of 1,3-diazin-4-ide or 1,3-diazin-2-ide match the observed spectrum. For a closer look at this agreement, Supporting Information Figure S1 shows the experimental spectrum overlaid with the simulations. The experimental spectral envelope is very regular, which is reproduced in the simulation of 1,3-diazin-5-ide. However, the predicted vibrational progressions of the 1,3-diazin-4-ide and 1,3-diazin-2-ide species are too broad and have very different vibrational structure. Furthermore, the calculated EA of the 1,3-diazin-5-ide isomer agrees very well with the measured value of 1.840 ± 0.006 eV, while the other isomers are calculated to have an EA more than half an eV lower—greater than our anticipated uncertainty for such a calculation. Thus, analysis of the simulated and experimental photoelectron spectra indicates that we observe the 1,3-diazin-5-ide isomer, and comparison of the calculated EA of each isomer to the measured EA of 1,3-diazinide confirms our assignment.

In addition, calculations of the $\Delta_{\text{acid}}H$ of each isomer support this assignment. The hydrogen at the 2-position is calculated to be much less acidic (at least 6 kcal mol^{-1}) than the other hydrogen atoms at the 4- and 5-positions and, therefore, will be inaccessible in our experiment. The measured $\Delta_{\text{acid}}H_{298}$ of $384.6 \pm 0.7 \text{ kcal mol}^{-1}$ is consistent with the calculated value of $383.7 \text{ kcal mol}^{-1}$ for the hydrogen at the 5-position, while the

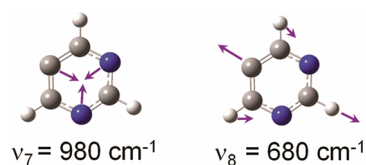
calculated value for the 4-position is $\sim 5 \text{ kcal mol}^{-1}$ higher than the measured value (see Table 4). Based on the agreement between the experimental and simulated photoelectron spectra, as well as the agreement of the measured $\Delta_{\text{acid}}H_{298}$ with calculations, it is clear that only 1,3-diazin-5-ide contributes to our measurements.

The regularity of the vibrational progression in Figure 3a is due to the fact that the spectrum is dominated by two vibrational progressions of the neutral 1,3-diazin-5-yl radical: 680 ± 20 and $980 \pm 20 \text{ cm}^{-1}$. In general, progressions observed in photoelectron spectroscopy arise from those vibrational modes with atomic displacements that reflect the greatest change in equilibrium geometry between the anion and the neutral species. The location of the excess electron in the anion has a large effect on the equilibrium geometry; in 1,3-diazin-5-ide, there is a lone pair of electrons on the 5-carbon atom. This causes the $\angle C_4C_5C_6$ bond angle to be smaller and the two adjacent C—C bonds to be longer than in the corresponding radical, which does not need to accommodate the excess charge. This prediction is confirmed by calculations that indicate a $+12.3^\circ$ change in the $\angle C_4C_5C_6$ bond angle, and a 0.035 \AA decrease in the adjacent C—C bond length upon photodetachment. These are the major deformations that occur upon radical formation. Therefore, we expect that the observed vibrational progressions will correspond to totally symmetric ring distortion vibrations that involve changes in the $\angle C_4C_5C_6$ bond angle and the C_4 — C_5 and C_6 — C_5 bond length. The substantial geometry change between the 1,3-diazin-5-ide anion and neutral 1,3-diazin-5-yl radical results in the observed extended vibrational progression spanning $\sim 1 \text{ eV}$.

Our calculations show that there are eight potentially active totally symmetric A_1 vibrational modes in 1,3-diazinyl radical. However, only two vibrational modes (ν_7 and ν_8) have sufficient displacements between anion and radical to make a significant contribution to the simulated photoelectron spectrum. The separation between the first and second and between the first and third peaks in the spectrum are similar to the calculated frequencies for these two modes. Therefore, provisional assignment of the first three peaks in the 1,3-diazin-5-ide spectrum correspond to the origin (0_0^0) and to the ν_8 and ν_7 fundamental transitions (8_0^1 and 7_0^1 , respectively); all calculated vibrational frequencies can be found in Supporting Information. In the 300 K spectrum (not shown), a hot band appears at lower binding energy from the origin, from which we measure a vibrational frequency of the anion: $660 \pm 40 \text{ cm}^{-1}$. The remaining peaks are either sequence or overtone bands. These two dominant active modes involve symmetric in-plane ring distortions, illustrated in Chart 1.

These two types of symmetric ring deformation modes are representative of the active modes in the other four azinyl systems, as well as phenyl,⁴⁵ and the measured frequencies in Table 2 are grouped accordingly. As described below, this provisional identification of the spectral features is confirmed by the simulation of the full photoelectron spectrum.

Chart 1



Both the experimental and simulated spectra of 1,3-diazin-5-ide show a well-resolved and nearly harmonic vibrational progression. The resolved structure is a consequence of the activity of only a few normal modes with non-overlapping vibrational progressions. The simulation confirms that most of the peaks in the photoelectron spectrum owe their intensity largely to single vibronic transitions (the red sticks in Figure 3b–d correspond to the Franck–Condon factors), and the resolved structure persists almost throughout the entire progression. The nearly equal peak spacing is in part due to the rigidity of the aromatic ring, leading to nearly harmonic vibrational modes. The excellent agreement between the experimental spectra and the Franck–Condon simulation using the independent harmonic-oscillator approximation indicates that the two active normal modes are predominantly uncoupled. The simulated spectrum most closely matches the experimental spectrum at low eBE because that is where the potential energy surface of the azinyl radical most closely resembles a harmonic oscillator; therefore, the independent-mode, harmonic-oscillator assumption is a reasonable approximation. However, we have found that even in much smaller molecular systems—such as dihalomethyl radicals (CHX_2)⁵⁰ and triplet states of the halocarbenes (CX_2)⁵¹—large geometry changes and “soft” vibrational potentials can lead to spectra that are congested and extremely difficult to assign quantitatively. When the simulation and experiment display near-quantitative agreement in structure and extent of the vibrational progression, the simulation can be used to identify the dominant active vibrational modes and to determine the vibronic transitions underlying peaks in the spectrum. Such is the case for all azinide anions reported here, confirming our assignment of the active vibrational modes.

Reactivity of 1,3-Diazine. The reactivity of 1,3-diazine is both complex and intriguing. When 1,3-diazine is deprotonated by HO^- , the proton affinity of the resulting anion is bracketed between the acidities of H_2O and CH_3OH . The anion also displays two H/D exchanges with D_2O , along with extremely slow deuterium abstraction ($\sim 3\%$). This result strongly suggests that 1,3-diazin-5-ide is the predominant anionic species arising from deprotonation by hydroxide, and that the 4-position of the 1,3-diazine is also sufficiently acidic for access to H/D exchange with D_2O . This is also consistent with the computational site-specific deprotonation enthalpies shown in Table 4. The amount of slow deuterium abstraction corresponds to the upper bound for 1,3-diazin-4-ide at 3%; thus, the only anion contributing significantly to our measurements is 1,3-diazin-5-ide.

Slow proton transfer is observed between 1,3-diazine and CH_3O^- . However, when 1,3-diazinide is generated in the source by deprotonation of 1,3-diazine with CH_3O^- , rather than with HO^- , a slightly different reactivity is observed; the anion reacts slightly less rapidly with methanol. When subjected to reaction with D_2O , a minor fraction of the anion resists H/D exchanges. Furthermore, the anions generated by deprotonation with HO^- and CH_3O^- exhibit different fragmentation patterns upon high energy SIFT injection. The C_2H^- (m/z 25) and CN^- (m/z 26) ions are the major products from the HO^- -generated anion, whereas a third unknown major fragment ion at m/z 51, is observed from the CH_3O^- -generated anion. These results suggest that the anion arising from deprotonation of 1,3-diazine by CH_3O^- contains a second ionic structure concurrently produced during the endoergic proton-transfer

reaction. We suspect the presence of a ring-opened 1,3-diazinide with a low proton affinity.

Gas-Phase Acidity of 1,3-Diazine. The forward reaction of 1,3-diazinide (generated by HO^- deprotonation) with CH_3OH produces CH_3O^- exclusively with the rate constant of $k_f = (12 \pm 2) \times 10^{-10} \text{ cm}^3 \text{ s}^{-1}$ (63% efficiency, $k_{\text{col}} = 19.3 \times 10^{-10}$). The overall rate of loss for the same reaction of 1,3-diazinide (but instead generated by CH_3O^-) with CH_3OH is slightly slower ($k_f = (10.7 \pm 0.3) \times 10^{-10} \text{ cm}^3 \text{ s}^{-1}$). This suggests that the CH_3O^- -generated A^- reagent anion contains $\sim 12\%$ of nonreactive species, presumably due to a ring-opened anion. This finding is in agreement with an estimate of $<18\%$ nonreactive species determined from the difference in H/D exchange ratios between the anions generated from either HO^- or CH_3O^- . The reverse reaction of 1,3-diazine with CH_3O^- is significantly slower ($\sim 5 \times 10^{-10} \text{ cm}^3 \text{ s}^{-1}$) and produced $\sim 30\%$ of A^- anion and $\sim 70\%$ of the $[\text{1,3-diazine} \cdots \text{CH}_3\text{O}^-]$ adduct, strongly suggesting an endoergic proton transfer.

Based on the reactivity studies for 1,3-diazinide generated in the source using CH_3O^- as the deprotonation agent, the A^- product anions contain $\sim 12\%$ of nonreactive species as byproduct. With a reasonable assumption that these byproducts arise from the ion–molecule complex that is endoergic with respect to proton transfer, the overall rate constant can be partitioned (70% adduct, 26% proton transfer, 4% ring-opened) to derive the effective rate constant for proton transfer, $k_r = (1.3 \pm 0.3) \times 10^{-10} \text{ cm}^3 \text{ s}^{-1}$ (5% efficiency, $k_{\text{col}} = 28.2 \times 10^{-10}$). Anchored by methanol, the acidity of 1,3-diazine at the 5-position was determined to be $\Delta_{\text{acid}}G_{298}(\text{1,3-diazine}) = 376.8 \pm 0.7 \text{ kcal mol}^{-1}$ and $\Delta_{\text{acid}}H_{298}(\text{1,3-diazine}) = 384.6 \pm 0.7 \text{ kcal mol}^{-1}$. Combining this enthalpy of deprotonation with the EA for 1,3-diazin-5-yl, we determine the C–H bond strength for the 5-position in 1,3-diazine to be $113.4 \pm 0.7 \text{ kcal mol}^{-1}$.

As mentioned earlier, very similar, albeit less complex, analyses were carried out for pyridine, 1,2-diazine, 1,4-diazine, and 1,3,5-triazine. The results are summarized below, with details similar to 1,3-diazine provided in the Supporting Information.

Pyridine. Pyridine has three possible anion isomers that result from deprotonation at the 2-, 3-, or 4-position: pyridin-2-ide, pyridin-3-ide, and pyridin-4-ide, respectively. Schafman and Wenthold measured similar gas-phase acidities of the hydrogen atoms at the 3- and 4-positions: $391.2\text{--}391.5$ and $389.9 \pm 2.0 \text{ kcal mol}^{-1}$, respectively.¹⁵ That study measured the regioselectivity of pyridine deprotonation under very similar experimental conditions to those used in this work and found 70–80% of the anions corresponded to pyridin-4-ide, and 20–30% corresponded to pyridin-3-ide.¹⁵ Deprotonation from the 2-position was shown to be inaccessible under their experimental conditions. Our FA-SIFT experiments found that the pyridinide anion exchanged two hydrogen atoms with D_2O , supporting the results of Schafman and Wenthold.¹⁵ These experimental results are consistent with the theoretical prediction (Table 4) that only the 3- and 4-position hydrogen atoms are sufficiently acidic to be accessed by HO^- . Thus, we do not expect to prepare pyridin-2-ide in our experiments, an expectation borne out in the simulations.

The photoelectron spectrum of pyridinide enables the identification of the deprotonation site. The experimental photoelectron spectrum of pyridinide is shown in Figure 4a, and the simulated spectra of the three possible anion isomers are plotted in Figure 4b–d. Because the EA that is measured in the experimental spectrum is unequivocal, all simulations are

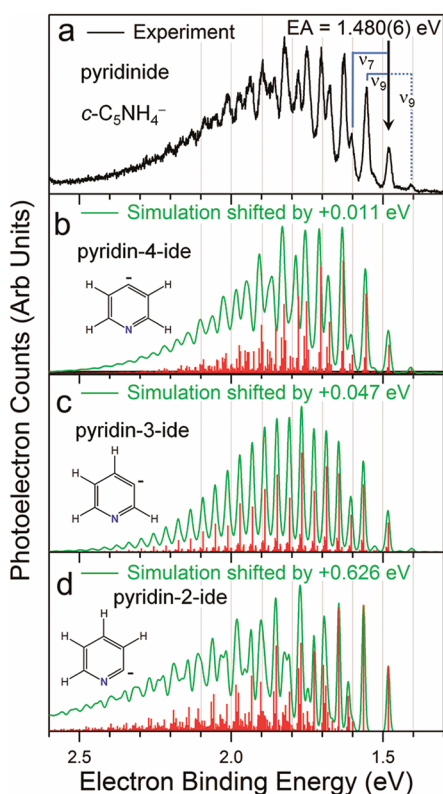


Figure 4. Magic-angle negative ion photoelectron spectra of pyridinide and simulations of possible anion isomers at 300 K: (a) 364-nm experimental spectrum; peaks used to identify vibrational frequencies are indicated with solid blue lines (neutral frequencies) and dashed blue lines (anion frequency). Simulated photoelectron spectra of pyridin-4-ide (b), pyridin-3-ide (c), and pyridin-2-ide (d) are plotted in green. Each simulation has been shifted by the difference between the experimental EA and the calculated EA of each isomer such that all simulations are plotted at the measured origin.

shifted by the difference between the measured EA and the calculated EA of each isomer such that the origin matches that of the observed spectrum. In this way we can readily compare the vibrational structure of the simulated and experimental spectra. The observed photoelectron spectrum displays near-quantitative agreement with the structure of the simulated spectrum of pyridin-4-ide (Figure S2 in Supporting Information shows the experimental spectrum overlaid with each simulation). Furthermore, the measured EA of pyridinyl is 1.480 ± 0.006 eV, in excellent agreement with the calculated EA of pyridin-4-yl, 1.469 eV. In contrast, the predicted spectrum of pyridin-3-ide, shown in Figure 4c, displays a much more regular vibrational progression than the experimental spectra. The simulated spectrum of pyridin-2-ide is shown in Figure 4d. We do not expect to see any signal from this isomer, as the 2-position is not sufficiently acidic to be deprotonated with HO^- ; indeed, the predicted spectrum is broader than that observed experimentally, and the calculated EA is substantially lower than the measured EA. Thus, we conclude that we predominantly observe signal from pyridin-4-ide, and the contribution from the pyridine-3-ide is less than 5%.

The measured EA of pyridin-4-yl is 1.480 ± 0.006 eV. We experimentally measure two vibrational frequencies of the pyridinyl radical, 600 ± 20 and 1010 ± 50 cm^{-1} , and one vibrational frequency of pyridinide anion, 580 ± 50 cm^{-1} (see

Table 2). Using the previously reported $\Delta_{\text{acid}}H$ and the measured EA, the C–H BDE for pyridine at the 4-position is 110.4 ± 2.0 kcal mol^{-1} .

1,2-Diazine. The measured 300 K photoelectron spectrum of 1,2-diazinide is shown in Figure 5a. The 1,2-diazine molecule

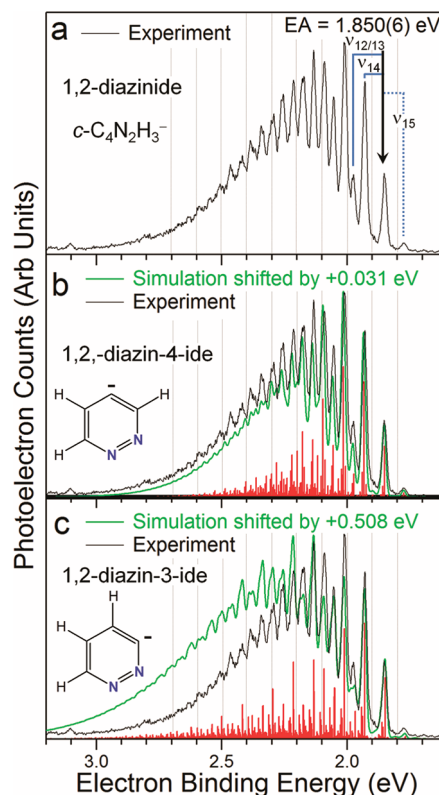


Figure 5. Magic-angle negative ion photoelectron spectra of 1,2-diazinide and simulations of possible anion isomers at 300 K: (a) 364-nm experimental spectrum; peaks used to identify vibrational frequencies are indicated with solid lines (neutral frequencies) and dashed lines (anion frequency). The simulated spectra for 1,2-diazin-4-ide and 1,2-diazin-3-ide are shown in (b) and (c), respectively. Each simulation has been shifted by the difference between the experimental EA and the calculated EA of each isomer such that all simulations are plotted at the measured origin.

has two unique hydrogen atoms with very different calculated acidities; the hydrogen at the 4-position is ~ 9 kcal mol^{-1} more acidic than the 3-position. Thus, we anticipate that we are more likely to deprotonate from the 4-position and form 1,2-diazin-4-ide in our experiments. The simulated spectra of 1,2-diazin-4-ide and 1,2-diazin-3-ide are presented in Figure 5b,c. Again, we will use both information about the active vibrational modes and the geometry change upon photodetachment (provided by the structure and extent of the vibrational progression), as well as the energy of the radical relative to the anion (given by the EA), to assign the isomer present in our experiments. So that we can readily compare the vibrational structure and extent of the progression, each simulation has been shifted by the difference between the measured EA and the calculated EA of each isomer such that each simulation is plotted with the experimental origin. Because the differences between the experimental and simulated spectra are especially subtle in this case, the experimental spectrum is overlaid in green (see Figure S3 for a full-page view of this comparison).

There is near-quantitative agreement in the vibrational structure between the experiment and the simulation of 1,2-diazin-4-ide. As with 1,3-diazin-5-ide, the simulation matches the observed spectrum most closely at low eBE, as that is where the independent harmonic-oscillator approximation employed in the Franck–Condon simulations is most valid. The simulation of 1,2-diazin-3-ide also displays similar vibrational structure near the onset of the progression as a result of the fact that similar vibrational modes of the 1,2-diazin-4-ide and 1,2-diazin-3-ide isomers are active upon photodetachment. However, the simulation of 1,2-diazin-3-ide is significantly broader than the observed spectrum, owing to the fact that the K'' displacements of the modes of the 1,2-diazin-3-ide isomer do not accurately represent the geometry change that takes place upon photodetachment. In addition, the calculated EA of 1,2-diazin-3-ide is significantly lower than the observed origin peak, providing further evidence that we only observe photoelectron signal from 1,2-diazin-4-ide.

The measured EA of 1,2-diazin-4-yl is 1.850 ± 0.006 eV. The photoelectron spectrum yields two vibrational frequencies for the 1,2-diazin-4-yl radical, 640 ± 20 and 1000 ± 80 cm^{-1} , and one frequency for 1,2-diazin-4-ide, 620 ± 50 cm^{-1} . Activity of the ν_{14} mode gives rise to the 640 cm^{-1} progression. Two totally symmetric modes (ν_{12} and ν_{13}) with nearly degenerate frequencies of ~ 1000 cm^{-1} and similar calculated intensities contribute to the spectrum. Based on the overall observed intensity of this transition, it is likely that both modes are active, and we report $\nu_{12} \approx \nu_{13} = 1000 \pm 80$ cm^{-1} .

The measured rate constants for the reaction of 1,2-diazin-4-ide with CH_3OH are $k_f = (2.2 \pm 0.4) \times 10^{-10}$ $\text{cm}^3 \text{s}^{-1}$ (11% efficiency, $k_{\text{col}} = 19.3 \times 10^{-10}$ $\text{cm}^3 \text{s}^{-1}$) and $k_r = (28 \pm 6) \times 10^{-10}$ $\text{cm}^3 \text{s}^{-1}$ (64% efficiency, $k_{\text{col}} = 43.6 \times 10^{-10}$). Using these values, we obtain a gas-phase acidity of $\Delta_{\text{acid}}G_{298}(1,2\text{-diazine}) = 374.0 \pm 0.7$ kcal mol^{-1} and a corresponding enthalpy of deprotonation of $\Delta_{\text{acid}}H_{298}(1,2\text{-diazine}) = 382.2 \pm 0.7$ kcal mol^{-1} . Three H/D exchanges were observed for 1,2-diazinide in reaction with D_2O . The results are rationalized by asserting that 1,2-diazin-4-ide is the predominant species, and that the 3-position is also sufficiently acidic to be available for H/D exchange. Combining the enthalpy of deprotonation measured above with the EA for 1,2-diazin-4-yl, we determine the C–H bond strength for the 4-position in 1,2-diazine to be 111.3 ± 0.7 kcal mol^{-1} .

1,4-Diazine. All four hydrogen atoms in 1,4-diazine are equivalent, so only one 1,4-diazinide isomer is possible upon deprotonation. The measured and simulated photoelectron spectra of 1,4-diazinide are given in Figure 6, and Figure S4 in Supporting Information shows the experimental spectrum overlaid with the simulation. Once again, the simulation has been shifted to the experimental origin to aid the comparison of experiment and simulation. The calculated geometry change is consistent with the observed spectrum, evidenced by the fact that the breadth of the simulation matches that of the experiment spectrum. The vibrational structure of the simulated spectrum displays good agreement with experiment, especially at low binding energy where the independent harmonic oscillator approximation is most valid, indicating that we correctly predict the harmonic frequencies of the vibrational modes active upon photodetachment. The measured EA of the 1,4-diazinyl radical is 1.254 ± 0.006 eV, again in good agreement with the calculated EA of 1.224 eV. We can experimentally identify two vibrational frequencies of the 1,4-diazinyl radical, 700 ± 20 and 980 ± 80 cm^{-1} , and one

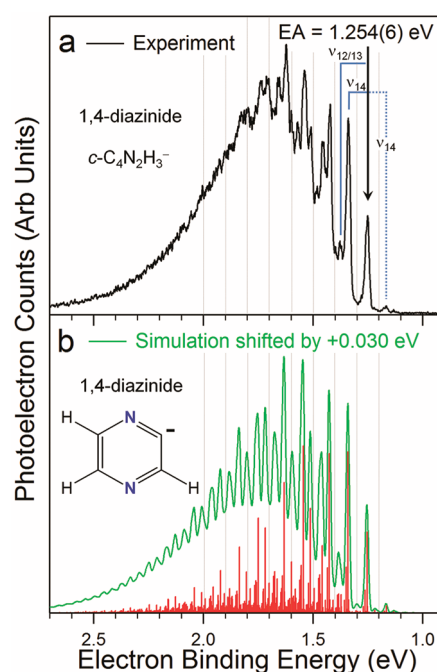


Figure 6. Magic-angle negative ion photoelectron spectrum of 1,4-diazinide: (a) 364-nm experimental spectrum with ions at 300 K. Peaks used to identify vibrational frequencies are indicated with solid (neutral frequency) and dashed lines (anion frequency). (b) Simulated photoelectron spectrum at 300 K. The simulation has been shifted by the difference between the experimental EA and the calculated EA such that the simulation is plotted at the measured origin.

frequency of the 1,4-diazinide anion, 670 ± 50 cm^{-1} . The dominant vibrational progression in the spectrum involves ring-deformation of the radical (ν_{14}), 700 ± 20 cm^{-1} . As was the case with 1,2-diazinide, the peaks in the ~ 980 cm^{-1} progression do not correspond to a single vibrational mode. There are two totally symmetric modes (ν_{12} and ν_{13}) that are calculated to have similar frequencies and intensities that both contribute the observed spectral features.

The rate constants for the reaction of 1,4-diazinide with H_2O are $k_f = (7.2 \pm 2) \times 10^{-10}$ $\text{cm}^3 \text{s}^{-1}$ (31% efficiency, $k_{\text{col}} = 23.3 \times 10^{-10}$) and $k_r = (9.3 \pm 2) \times 10^{-10}$ $\text{cm}^3 \text{s}^{-1}$ (51% efficiency, $k_{\text{col}} = 18.3 \times 10^{-10}$). Using the gas-phase acidity of water, the acidity of 1,4-diazine is $\Delta_{\text{acid}}G_{298}(1,4\text{-diazine}) = 383.5 \pm 0.4$ kcal mol^{-1} , with a corresponding enthalpy of deprotonation $\Delta_{\text{acid}}H_{298}(1,4\text{-diazine}) = 392.2 \pm 0.4$ kcal mol^{-1} . Three sites in 1,4-diazinide rapidly undergo H/D exchange with D_2O . These results show that the equivalent C–H sites in 1,4-diazine have an acidity very close to that of water. From the measured enthalpy of deprotonation with the EA for 1,4-diazinyl, the C–H bond strength for 1,4-diazine is found to be 107.5 ± 0.4 kcal mol^{-1} .

1,3,5-Triazine. The three hydrogen atoms in 1,3,5-triazine are equivalent, and deprotonation yields only one 1,3,5-triazinide isomer. The experimental photoelectron spectrum for 1,3,5-triazinide is shown in Figure 7a, along with the Franck–Condon simulation shifted to the experimental origin (Figure 7b). The simulated spectrum shows excellent agreement with the measured photoelectron spectrum in both the vibrational structure and the extent of the progression (see also Figure S5 to view the experimental spectrum overlaid with the simulation). The measured EA of 1,3,5-triazinyl is 1.529 ± 0.006 eV, which is consistent with the calculated EA. The

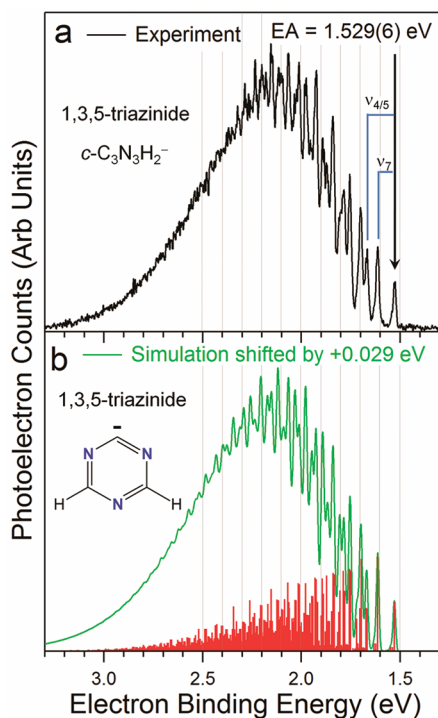


Figure 7. Magic-angle negative ion photoelectron spectrum of 1,3,5-triazinide: (a) 364-nm experimental spectrum with ions cooled to ~ 150 K. Peaks used to identify vibrational frequencies are indicated with solid lines. (b) Simulated photoelectron spectrum at 150 K. The simulation has been shifted by the difference between the experimental EA and the calculated EA such that the simulation is plotted at the measured origin.

excellent agreement between simulation and experiment allows for identification of the peaks in the spectrum. We measure two vibrational frequencies for the 1,3,5-triazinyl radical, 680 ± 20 and 1110 ± 70 cm^{-1} , and one frequency for 1,3,5-triazinide anion, 670 ± 40 cm^{-1} . As with 1,2-diazinyl, two modes (ν_4 and ν_5) with nearly degenerate frequencies of ~ 1100 cm^{-1} contribute to the observed spectrum.

The rate constant for the reaction of 1,3,5-triazinide with CH_3OH is $k_f = (11 \pm 2) \times 10^{-10}$ $\text{cm}^3 \text{s}^{-1}$ (53% efficiency, $k_{\text{col}} = 19.3 \times 10^{-10}$). For the reverse reaction of 1,3,5-triazine with CH_3O^- , we consider possible ring-open structures (mechanistic details discussed elsewhere¹⁶) as well as impurities and obtain a conservative estimate, $k_r = (0.55 \pm 0.20) \times 10^{-10}$ $\text{cm}^3 \text{s}^{-1}$ (4% efficiency, $k_{\text{col}} = 13.7 \times 10^{-10}$). From the gas-phase acidity of methanol, we determine the acidity of 1,3,5-triazine to be $\Delta_{\text{acid}}G_{298}(\text{1,3,5-triazine}) = 377.3 \pm 0.7$ kcal mol^{-1} , and the corresponding enthalpy of deprotonation is $\Delta_{\text{acid}}H_{298}(\text{1,3,5-triazine}) = 386.1 \pm 0.7$ kcal mol^{-1} . Slow H/D exchange was observed for two sites on 1,3,5-triazinide with D_2O . These results indicate that there is a moderate basicity gap between the anion and HO^- (~ 10 kcal mol^{-1}), and the three equivalent hydrogen atoms are more acidic than water. Combining the enthalpy of deprotonation with the EA for 1,3,5-triazinyl, the C–H bond strength for 1,3,5-triazine is found to be 107.8 ± 0.7 kcal mol^{-1} .

DISCUSSION

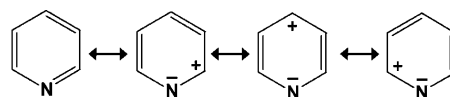
To better understand the chemical effects of replacing CH groups with nitrogen atoms in six-membered rings, we first compare pyridine with benzene; this is the simplest case, where

only one nitrogen atom has been added. The other molecules included in this work (the diazines and 1,3,5-triazine) form a series in which nitrogen atoms are added and displaced throughout the ring, yielding insight into the influence of heteroatom substitution on thermochemistry.

Our experiments determine three key thermochemical properties for each species: $\Delta_{\text{acid}}H$ for the most acidic site of the neutral molecule, the EA of the corresponding radical, and the C–H BDE at the deprotonation site. These values are related through the negative ion thermochemical cycle (shown in Figure 2), and we will focus our discussion on two quantities: the $\Delta_{\text{acid}}H_{298}$ and C–H BDE. These values most directly represent the stability of an azinide anion and the azinyl radical, respectively, relative to the parent azine compound. The stability of the anions and the radicals depends on the presence and location of the electronegative nitrogen atom(s) in the ring. In general, there are two main competing electronic effects that contribute to the thermochemical properties of aromatic molecules and their radicals: an inductive effect assisted by resonance^{52,53} and electron lone-pair repulsion in nearest-neighbor sites.^{9,11,12,54} Azinide anions, formed by deprotonation of a parent azine molecule, have electron pairs created at the deprotonation site, oriented in the plane of the ring. Therefore, the anion stability should be quite sensitive to both of these effects. In contrast, azinyl radicals have an *unpaired* electron in the plane of the ring; their stability should still depend on inductive and resonance effects, but it will be less sensitive to the nearest-neighbor repulsion.

These competing effects are clearly manifested in pyridine. Like benzene, pyridine is aromatic, with one C–H group replaced by an electronegative nitrogen atom that contains a lone pair of electrons in an in-plane sp^2 -hybridized orbital. This substitution causes the hydrogen atoms in the 2-, 3-, and 4-positions—*ortho*, *meta*, and *para* respectively—to have different acidities, depending on their proximity to the nitrogen atom.¹⁵ Forming the anion at the *para* position is favored due to resonance-assisted stabilization, depicted in Scheme 1.

Scheme 1



Specifically, resonance structures of pyridine place a positive charge at the *ortho* and *para* positions; thus, deprotonation from the *ortho* and *para* positions is favored because the negative charge of the anion is stabilized by electrostatic interaction with the positive charge. Furthermore, the electronegative nitrogen withdraws electron density from the anion through the sigma bonding framework via the inductive effect, delocalizing the excess charge of the anion.^{52,53} However, the *ortho* position suffers from significant electron-pair repulsion with the lone-pair electrons on the nitrogen atom, destabilizing the anion. As a result, the hydrogen atom in the *para* position is the most acidic, and the deprotonation enthalpy of pyridine is 11.3 kcal mol^{-1} less than benzene (see Table 1).

The experiments show that the strength of the C–H bond at the *para* position in pyridine is 110.4 ± 2 kcal mol^{-1} , only slightly less than that of benzene (112.9 ± 0.5 kcal mol^{-1}). This result reflects the lack of significant electronic interaction between the unpaired electron at the deprotonation site and the nitrogen atom in pyridin-4-yl. Electron repulsion should not be

an important interaction for unpaired electrons in general, and the separation of the radical site and the nitrogen atom by two carbon atoms minimizes any charge delocalization via the inductive effect between them. Previous studies on pyridin-2-yl suggest that a radical adjacent to a nitrogen atom can be stabilized by an inductive interaction between the in-plane unpaired electron and the adjacent nitrogen lone pair.^{9,11,12,54} This picture is fully consistent with the previously measured C–H bond strength at the *ortho* position of pyridine, which is lower than the other two positions by 7 kcal mol^{−1}.¹¹

In summary, insertion of a single nitrogen atom into a benzene ring leads to a lower enthalpy of deprotonation but does not greatly affect the C–H bond strength at the *para* position in pyridine. Consequently, the EA of pyridin-4-yl radical is 1.480 ± 0.006 eV, an ~50% increase (or ~9 kcal mol^{−1}) from the EA of the phenyl radical, 1.096 ± 0.006 eV.

Examination of the other azines in this study reveals the effects of increasing nitrogen content in an aromatic system. Looking first at the radical stability, we see that the simple chemical picture outlined above generally applies quite well. The two most straightforward cases are 1,4-diazine and 1,3,5-triazine, as all hydrogen atoms in these molecules are equivalent. Both 1,4-diazine and 1,3,5-triazine have C–H bond strengths lower than that of benzene and pyridine (see Table 1), owing to the radical stabilization by nearest-neighbor nitrogen atoms. On the other hand, in 1,2-diazine and 1,3-diazine, the experiments probe deprotonation sites that are not adjacent to nitrogen atoms; consequently, the C–H bond strengths are again similar to pyridine and benzene, showing no significant radical stabilization.

Turning to the anion stability in species with multiple nitrogen atoms, we again find evidence of competing electronic effects: an inductive effect assisted by resonance and lone-pair repulsion (Table 1). The most acidic sites of all the azines studied have $\Delta_{\text{acid}}H$ values lower than that of benzene, showing net anion stabilization coinciding with the addition of nitrogen atoms; however, not all species follow a clear trend. Analysis of the pyridine data suggests that the carbon site *para* to a nitrogen atom forms the most stable anion and therefore contains the most acidic proton. Indeed, only 1,4-diazine has no available *para* deprotonation site, and it exhibits a $\Delta_{\text{acid}}H$ higher than the measured value for pyridine at the *para* position. The most acidic site in 1,2-diazine, *meta* and *para* to the nitrogen atoms, is subject to resonance-assisted stabilization without lone-pair repulsion, and therefore 1,2-diazine has the lowest $\Delta_{\text{acid}}H$ value of all species surveyed. We expect 1,3,5-triazine to have extensive resonance-assisted electrostatic stabilization, combined with strong repulsive interactions due to two nearest-neighbor nitrogen atoms. On the balance, it has a slightly lower $\Delta_{\text{acid}}H$ value than pyridine at the *para* position. Finally, the most acidic site in 1,3-diazine is the 5-position, *meta* to both nitrogen atoms.

As noted previously, one of the motivating factors for undertaking this study was to obtain experimental BDE values to serve as benchmarks in the evaluation of computational methods. In 1999, Barckholtz et al. published a thorough computational study of the C–H and N–H BDEs of small aromatic hydrocarbons.¹⁷ Judging by the agreement with the available experimental BDEs, they concluded that the B3LYP level of theory adequately predicts thermochemical properties and BDEs of aromatic hydrocarbons. In support of their findings, our B3LYP calculated thermochemical values, summarized in Table 4, agree well with our experimental

measurements, which are limited to anions formed at the most acidic deprotonation site in the azine ring. This agreement, along with the results of the computational study,¹⁷ gives us confidence to use the calculated values for other C–H sites to obtain additional insight into azine thermochemistry. For example, the 1,3,5-triazinyl radical differs from the 1,3-diazin-2-yl radical by a nitrogen substitution in the position *para* to the radical site. This results in the C–H BDE being roughly the same, but the $\Delta_{\text{acid}}H$ value is ~10 kcal mol^{−1} smaller, and EA is ~10 kcal mol^{−1} larger. This indicates that a nitrogen atom *para* to the radical site in 1,3,5-triazine increases the anion stability (compared to 1,3-diazine), consistent with the findings from pyridine.

Based on the experimental observations and the calculated values in Table 4, we make several additional observations concerning the thermochemistry of azines. In general, the proximity of the C–H bond or anion/radical site to nitrogen atoms has a greater effect on the measured thermochemical values than does the total number of nitrogen substitutions. The effect on anion stability is stronger than on radical stability; the measured $\Delta_{\text{acid}}H$ values in Table 4 vary by as much as 19 kcal mol^{−1}, while all of the measured C–H BDEs span a narrower range: only 6 kcal mol^{−1}. In agreement with the Barckholtz et al. study, we find that the C–H bonds are weakest when adjacent to a nitrogen atom—a result of the delocalization of the unpaired electron¹⁷—and strongest when farther from a nitrogen atom. Lastly, the most acidic site in the azine ring corresponds to the strongest C–H bond (the largest BDE value).

CONCLUSION

Five azine molecules were investigated using both negative ion photoelectron spectroscopy and ion kinetics using a FA-SIFT reactor. We report EAs for the five azinyl radicals that result from the removal of a hydrogen atom from the most acidic site of the corresponding azine, and we greatly improve the accuracy of the deprotonation enthalpies for four of the studied azine molecules. The photoelectron spectra of the five azines have very similar vibrational progressions and frequencies, a consequence of the very similar geometric distortions that occur upon electron addition to the radical. The measured acidities and EAs can be rationalized by electrostatic arguments, as certain anion sites are preferentially stabilized by the inductive effect assisted by resonance, while others are destabilized by electron-pair repulsion. However, as the nitrogen content increases in the diazines and 1,3,5-triazine, a balancing of these competing effects is manifested in our results. We determine site-specific BDE values for all five azines. The results show that the proximity of the C–H bond relative to a nitrogen atom has a greater influence on the thermochemistry (EA, BDE, $\Delta_{\text{acid}}H_{298}$) than the number of nitrogen atoms in the azine. Furthermore, we find that C–H bonds adjacent to a nitrogen atom have lower BDEs relative to C–H bonds *meta* or *para* to the nitrogen.

ASSOCIATED CONTENT

Supporting Information

Figures S1–S5, experimental azinide spectra overlaying the simulations of the various possible isomers, as well as a detailed discussion of each isomer assignment; Tables S1–S5, calculated vibrational frequencies for azinide anions and corresponding azinyl radicals; complete ref 38. This material is available free of charge via the Internet at <http://pubs.acs.org>.

■ AUTHOR INFORMATION

Corresponding Author

veronica.bierbaum@colorado.edu; wcl@jila.colorado.edu

Present Addresses

[†]Department of Chemistry, United States Air Force Academy, Colorado Springs, CO 80840

[‡]Combustion Research Facility, Sandia National Laboratories, Livermore, California 94551, United States

Notes

The authors declare no competing financial interest.

■ ACKNOWLEDGMENTS

We are pleased to acknowledge generous support from the Air Force Office of Scientific Research (Grant FA9550-09-1-0046) and the National Science Foundation (Grants CHE-0809391 (W.C.L.) and CHE-1012321 (V.M.B.)). J.M.G. respectfully acknowledges the sponsorship and support of the Air Force Institute of Technology. We are also grateful to G. B. Ellison for his enlightening discussions, as well as JILA Visiting Fellows R. J. McMahon and D. L. Osborn for their insight on this work.

■ REFERENCES

- (1) *The Structure and Reaction Processes of Coal*; Smith, K. L., Smoot, L. D., Fletcher, T. H., Pugmire, R. J., Eds.; Plenum Press: New York, 1994.
- (2) Wallace, S.; Bartle, K. D.; Perry, D. L. *Fuel* **1989**, *68*, 1450.
- (3) Hore, N. R.; Russell, D. K. *J. Chem. Soc., Perkin Trans. 2* **1998**, 269.
- (4) Axworthy, A. E.; Dayan, V. H.; Martin, G. B. *Fuel* **1978**, *57*, 29.
- (5) Pohl, J. H.; Sarofim, A. F. *Symp. (Int.) Combust.* **1977**, *16*, 491.
- (6) Fried, L. E.; Manaa, M. R.; Pagoria, P. F.; Simpson, R. L. *Annu. Rev. Mater. Res.* **2001**, *31*, 291.
- (7) Turker, L.; Gumus, S.; Atalar, T. *J. Energetic Mater.* **2010**, *28*, 139.
- (8) FinlaysonPitts, B. J.; Pitts, J. N. *Science* **1997**, *276*, 1045.
- (9) Doughty, A.; Mackie, J. C. *J. Chem. Soc., Faraday Trans.* **1994**, *90*, 541.
- (10) Jones, J.; Bacskey, G. B.; Mackie, J. C.; Doughty, A. *J. Chem. Soc., Faraday Trans.* **1995**, *91*, 1587.
- (11) Kiefer, J. H.; Zhang, Q.; Kern, R. D.; Yao, J.; Jursic, B. *J. Phys. Chem. A* **1997**, *101*, 7061.
- (12) Mackie, J. C.; Colket, M. B.; Nelson, P. F. *J. Phys. Chem.* **1990**, *94*, 4099.
- (13) Mackie, J. C.; Colket, M. B.; Nelson, P. F.; Esler, M. *Int. J. Chem. Kinet.* **1991**, *23*, 733.
- (14) Xu, H.; Kiefer, J. H. *Int. J. Chem. Kinet.* **2010**, *42*, 211.
- (15) Schafman, B. S.; Wenthold, P. G. *J. Org. Chem.* **2007**, *72*, 1645.
- (16) Garver, J. M.; Yang, Z.; Kato, S.; Wren, S. W.; Vogelhuber, K. M.; Lineberger, W. C.; Bierbaum, V. M. *J. Am. Soc. Mass Spectrom.* **2011**, *22*, 1260.
- (17) Barckholtz, C.; Barckholtz, T. A.; Hadad, C. M. *J. Am. Chem. Soc.* **1999**, *121*, 491.
- (18) Henry, G. D. *Tetrahedron* **2004**, *60*, 6043.
- (19) Ancil, E. J.-G.; Snieckus, V. In *Metal-Catalyzed Cross-Coupling Reactions*, 2nd ed.; De Meijere, A., Diederich, F., Eds.; Wiley-VCH: Weinheim, 2004; p 761.
- (20) Martin, R.; Buchwald, S. L. *Acc. Chem. Res.* **2008**, *41*, 1461.
- (21) Surry, D. S.; Buchwald, S. L. *Angew. Chem., Int. Ed.* **2008**, *47*, 6338.
- (22) Lyons, T. W.; Sanford, M. S. *Chem. Rev.* **2010**, *110*, 1147.
- (23) Chen, X.; Engle, K. M.; Wang, D. H.; Yu, J. Q. *Angew. Chem., Int. Ed.* **2009**, *48*, 5094.
- (24) Ervin, K. M.; DeTuro, V. F. *J. Phys. Chem. A* **2002**, *106*, 9947.
- (25) Blanksby, S. J.; Ellison, G. B. *Acc. Chem. Res.* **2003**, *36*, 255.
- (26) Ervin, K. M.; Lineberger, W. C. In *Advances in Gas Phase Ion Chemistry*; Adams, N. G., Babcock, L. M., Eds.; JAI Press: Greenwich, CT, 1992; Vol. 1, p 121.
- (27) Neumark, D. M.; Lykke, K. R.; Andersen, T.; Lineberger, W. C. *Phys. Rev. A* **1985**, *32*, 1890.
- (28) Ervin, K. M.; Anusiewicz, W.; Skurski, P.; Simons, J.; Lineberger, W. C. *J. Phys. Chem. A* **2003**, *107*, 8521.
- (29) Cooper, J.; Zare, R. N. *J. Chem. Phys.* **1968**, *48*, 942.
- (30) Van Doren, J. M.; Barlow, S. E.; DePuy, C. H.; Bierbaum, V. M. *Int. J. Mass Spectrom. Ion Processes* **1987**, *81*, 85.
- (31) Bierbaum, V. M. In *Encyclopedia of Mass Spectrometry*; Gross, M. L., Caprioli, R., Eds.; Elsevier: Amsterdam, 2003; Vol. 1, p 276.
- (32) Davico, G. E.; Bierbaum, V. M.; DePuy, C. H.; Ellison, G. B.; Squires, R. R. *J. Am. Chem. Soc.* **1995**, *117*, 2590.
- (33) Gianola, A. J.; Ichino, T.; Hoeningman, R. L.; Kato, S.; Bierbaum, V. M.; Lineberger, W. C. *J. Phys. Chem. A* **2005**, *109*, 11504.
- (34) Gianola, A. J.; Ichino, T.; Kato, S.; Bierbaum, V. M.; Lineberger, W. C. *J. Phys. Chem. A* **2006**, *110*, 8457.
- (35) Su, T.; Chesnavich, W. J. *J. Chem. Phys.* **1982**, *76*, 5183.
- (36) *CRC Handbook of Chemistry and Physics*, 92nd ed.; Haynes, W. M., Ed.; CRC Press/Taylor and Francis: Boca Raton, FL, 2011.
- (37) Miller, K. J.; Savchik, J. A. *J. Am. Chem. Soc.* **1979**, *101*, 7206.
- (38) Frisch, M. J. et al. *Gaussian 03*, Revision B.05; Gaussian, Inc.: Pittsburgh, PA, 2003.
- (39) Becke, A. D. *J. Chem. Phys.* **1993**, *98*, 5648.
- (40) Lee, C. T.; Yang, W. T.; Parr, R. G. *Phys. Rev. B* **1988**, *37*, 785.
- (41) Woon, D. E.; Dunning, T. H. *J. Chem. Phys.* **1993**, *98*, 1358.
- (42) Dunning, T. H. *J. Chem. Phys.* **1989**, *90*, 1007.
- (43) Ervin, K. M. *PESCAL*, Fortran program, 2010.
- (44) Ervin, K. M.; Ramond, T. M.; Davico, G. E.; Schwartz, R. L.; Casey, S. M.; Lineberger, W. C. *J. Phys. Chem. A* **2001**, *105*, 10822.
- (45) Gunion, R. F.; Gilles, M. K.; Polak, M. L.; Lineberger, W. C. *Int. J. Mass Spectrom. Ion Processes* **1992**, *117*, 601.
- (46) Ervin, K. M.; Gronert, S.; Barlow, S. E.; Gilles, M. K.; Harrison, A. G.; Bierbaum, V. M.; DePuy, C. H.; Lineberger, W. C.; Ellison, G. B. *J. Am. Chem. Soc.* **1990**, *112*, 5750.
- (47) Ichino, T.; Gianola, A. J.; Kato, S.; Bierbaum, V. M.; Lineberger, W. C. *J. Phys. Chem. A* **2007**, *111*, 8374.
- (48) Villano, S. M.; Eyet, N.; Wren, S. W.; Ellison, G. B.; Bierbaum, V. M.; Lineberger, W. C. *Eur. J. Mass Spectrom.* **2010**, *16*, 255.
- (49) Villano, S. M.; Eyet, N.; Wren, S. W.; Ellison, G. B.; Bierbaum, V. M.; Lineberger, W. C. *J. Phys. Chem. A* **2010**, *114*, 191.
- (50) Vogelhuber, K. M.; Wren, S. W.; McCoy, A. B.; Ervin, K. M.; Lineberger, W. C. *J. Chem. Phys.* **2011**, *134*, 184306.
- (51) Wren, S. W.; Vogelhuber, K. M.; Ervin, K. M.; Lineberger, W. C. *Phys. Chem. Chem. Phys.* **2009**, *11*, 4745.
- (52) Hammett, L. P. *Physical Organic Chemistry*; McGraw-Hill: New York, 1940.
- (53) Hine, J. *Physical Organic Chemistry*; McGraw-Hill: New York, 1962.
- (54) Kikuchi, O.; Hondo, Y.; Morihashi, K.; Nakayama, M. *Bull. Chem. Soc. Jpn.* **1988**, *61*, 291.